ORIGINAL ARTICLE

Errors in Thermographic Camera Measurement Caused by Known Heat Sources and Depth Based Correction

Mark Christian E. Manuel[1], Shu-Ping Lin[1], Wei-Hao Lu[1], and Po Ting Lin[1,*]

[1]*Department of Mechanical Engineering at Chung Yuan Christian University, Chungli, Taoyuan, Taiwan*

(**Received** 18 October 2015; **Accepted** 10 December 2015; **Published on line** 1 March 2016)

*Corresponding author: potinglin@cycu.edu.tw

DOI: 10.5875/ausmt.v6i1.1003

Abstract: Thermal imaging has shown to be a better tool for the quantitative measurement of temperature than single spot infrared thermometers. However, thermographic cameras can encounter errors in acquiring accurate temperature measurements in the presence of other environmental heat sources. Some of these errors arise due to the inability of the thermal camera to detect objects and features in the infrared domain. In this paper, the thermal image is registered as a stereo image from a Kinect system prior to depth-based correction. Experiments demonstrating the error are presented together with the determination of the measurement errors under prior knowledge of the thermographed scene. The proposed correction scheme improves the accuracy of the thermal image through augmentation using the Kinect system.

Keywords: stereo vision, Kinect, infrared thermography, radiation

Introduction

Thermal imaging devices or thermographic cameras were originally used to conduct qualitative measurements such as for seeking objects or detecting hot spots [1]. However, their ability to create a two-dimensional temperature map of a scene offers the possibility of better and more detailed quantification compared to that of a single spot IR thermometer. Recent technological improvements in the construction, components and sensors of thermal imaging devices have led to their increased commercial use across multiple sectors and disciplines at lower costs [2]. Quantitative thermal imaging requires that a true temperature value be assigned to each pixel in the image, and is subject to problems unique to infrared thermography. Key issues include reflections from surrounding objects, knowledge of surface emissivity, and the size-of-source effect [3]. The temperature of one object can be accurately measured by a thermographic camera without radiation interference from other ambient heat sources. However, temperature measurement errors may occur when the thermal radiation of the surroundings is reflected onto the measured object and is thus captured by the thermal camera. The reflected thermal radiation could be quantified, but is subject to the same problem of reflection and knowledge of surface emissivity, which thermographic camera are poorly equipped to deal with. These errors could be corrected if the thermographic camera can detect objects and features. However, thermographic camera measurements are mostly performed in the infrared (IR) spectrum where features such as shape and boundary are not as easily distinguishable as in the visible spectrum. In addition, most research into thermal imaging and related applications are based on two-dimensional images of a scene, whereas the factors affecting thermal images are three-dimensional.

Several studies have proposed a variety of 3D thermographic techniques. Chen et al. [4] recently proposed a 3D infrared imaging approach based on silhouette volume intersection to reconstruct volumetric temperature data of enclosed objects. Multiple IR images are taken from various angles and integrated with 2D RGB

images to effectively reconstruct a 3D model of the object's temperature distributions. De Souza et al. [5] introduced a new method to combine 2D Infrared Images with Magnetic Resonance Images (MRI) and/or Computer Tomography (CT) images using an image registration methodology. Ng and Du [6] reconstructed an object's 3D thermal distribution using the octave carving technique. Xiao et al. [7] used structured light for 3D profiling, using a He-Ne laser projector with a thermal and a digital CCD. Bakker et al. [8] used a single thermal camera with a stimulation of thermal pulses from high power lamps. A similar approach was used by Maldague [9] who coined the term "shape-from-heating" as the object's shape is inferred from the observed temperature decay of the pulsed transient IR images.

Prakash et al. [10] demonstrated two different stereo methods for the 3D mapping of an object's temperatures: visual stereo and thermal stereo. Their visual stereo system consists of two cameras and one thermal camera and follows a sequential method wherein the geometry needs to be reconstructed first and the temperature information is then mapped to the point clouds. The thermal stereo system uses two different thermal cameras; the isotherms of each image are used for geometric reconstruction therefore mooting the need for temperature information in the generated point clouds. This study uses the visual stereo system since we know that isotherms obtained from a thermal camera may include errors when taken in the presence of other heat sources. Yang and Chen [11] greatly improved the accuracy of the visual stereo system by integrating structured light with a pixel accuracy of up to 10 μm and by highlighting the calibration of such systems. To our knowledge, none of these studies on thermal stereovision discussed error correction on the obtained thermographic images or used the Kinect system as the 3D mapping system. Thus, this paper presents the use of Kinect to first identify objects in the thermographed scene. Using Kinect provides several advantages over a built stereovision system including increased ease of use, improved calibration (thus removing the need for extensive calibration procedures), low cost and accurate depth maps which conveniently output as RGBD images. After objects are identified, the temperature data from the thermographic image is assigned to the generated cloud points. Correction filters from prior knowledge that the objects are isothermal are then applied. The correction filters contain information about the error from a known heat source.

The remainder of this paper is as follows. Section two discusses thermography errors for which the proposed scheme is design to compensate. This initial work is based on the assumption that all of the objects in the thermographed scene are isothermal and that their temperatures are verified using thermocouples. Section three discusses the Kinect system used. Section four describes the experimental set-up and the results of the corrected 3D temperature data reconstructed using the Kinect system.

Mark Christian E. Manuel is a PhD student in Department of Mechanical Engineering at Chung Yuan Christian University, Chungli, Taoyuan, Taiwan 32023.

Shu-Ping Lin is a MS student in Department of Mechanical Engineering at Chung Yuan Christian University, Chungli, Taoyuan, Taiwan 32023.

Wei-Hao Lu is a MS student in Department of Mechanical Engineering at Chung Yuan Christian University, Chungli, Taoyuan, Taiwan 32023.

Po Ting Lin is an Associate Professor in Department of Mechanical Engineering at Chung Yuan Christian University, Chungli, Taoyuan, Taiwan 32023. He is also with Research Center for Microsystem Engineering and Center for Robotics Research at Chung Yuan Christian University.

Infrared Thermography

Principles of Infrared Thermography

Any object at a temperature above absolute zero emits infrared radiation and the amount of radiation emitted increases with radiation [12]. Infrared thermography is a method used to detect the infrared energy emitted from an object, which is related to an object's temperature. Typically, infrared thermography devices or thermographic cameras are designed and calibrated for the range of the infrared (IR) spectrum, which lies between visible light and microwaves within a wavelength spectrum of 0.7 – 1000 mm (see Fig. 1). The IR spectrum is further subdivided into several spectral regions: near infrared (NIR), short wavelength infrared (SWIR), mid-wavelength infrared (MWIR), long-wavelength infrared (LWIR) and very long wavelength infrared (VLWIR) or far-infrared [13].

The break between MWIR and LWIR is caused by the absorption of the other wavelengths by molecules in the atmosphere, mainly by CO2 and H2O. NIR and SWIR are often referred to as reflected IR. The MWIR and the LWIR are referred as thermal infrared (TIR) since they cover objects that are in the range of 190K-1000K.

The radiation caused by an object's temperature, T, is described by Planck's wavelength distribution function, typically known as Planck's Law [14] and is mathematically expressed as:

$$I(\lambda,T)=\frac{2\pi hc^2}{\lambda^5\exp(hc/\lambda k_B T-1)} \quad (1)$$

where $I(\lambda,T)$ is the electromagnetic radiation intensity emitted as a function of wavelength and absolute temperature, λ is the wavelength, h is Planck's constant (6.626×10^{-34} Js), c is the speed of light (2.997

$\times$ 10^8 m/s) and k_B is the Boltzmann's constant (1.3806503 $\times$ 10^{-23} J/K). Figure 2 from [15] shows the radiation emitted by a black body.

Observations for this function tell us that the maximum electromagnetic radiation intensity for each temperature peaks at different wavelengths. The relationship between them is inversely proportional and can be calculated by Wien's Law, as given in Eq. (2). We can also observe that most of the radiation of a high temperature object is in MWIR, while the radiation emitted by low temperature objects is mostly in the LWIR.

$$\lambda_{peak} = \frac{0.0029[m/K]}{T} \quad (2)$$

The total hemispherical radiation intensity is calculated by integrating Planck's Law through all wavelengths. It is simplified in the Stefan-Boltzmann formula given by Eq. (3). This is the theoretical amount of power emitted by a blackbody as a function of its temperature alone.

$$\dot{Q}_{rad,B} = \sigma A T^4 \quad (3)$$

where $\dot{Q}_{rad,B}$ is the maximum emissive power of a perfect blackbody, and σ is the Stefan-Boltzmann constant (5.670373 $\times$ 10^{-8} W/m^{2}K^4).

A real body emits only a fraction of the thermal energy emitted by a blackbody at the same temperature. If the object is colder than about 500°C, the emitted radiation lies completely within IR wavelengths [16]. A body's emissivity is formally defined for a wavelength as the ratio of the radiant energy emitted by the body to the radiation that would be emitted by a blackbody at the same temperature. If the emissivity is constant and independent of the wavelength, the body is said to be a grey body. The emissivity of a grey body can be mathematically expressed as:

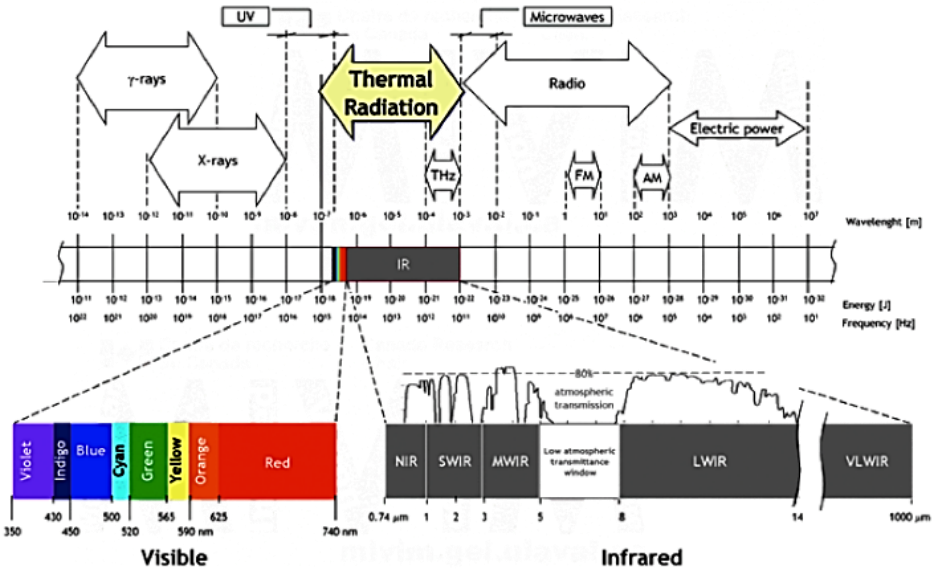

Figure 1. Electromagnetic spectrum with subdivided visible and infrared regions. IR region reflects typical atmospheric transmission. (Source: https://en.wikipedia.org/wiki/Infrared_vision#/media/File:Infrared_spectrum.gif)

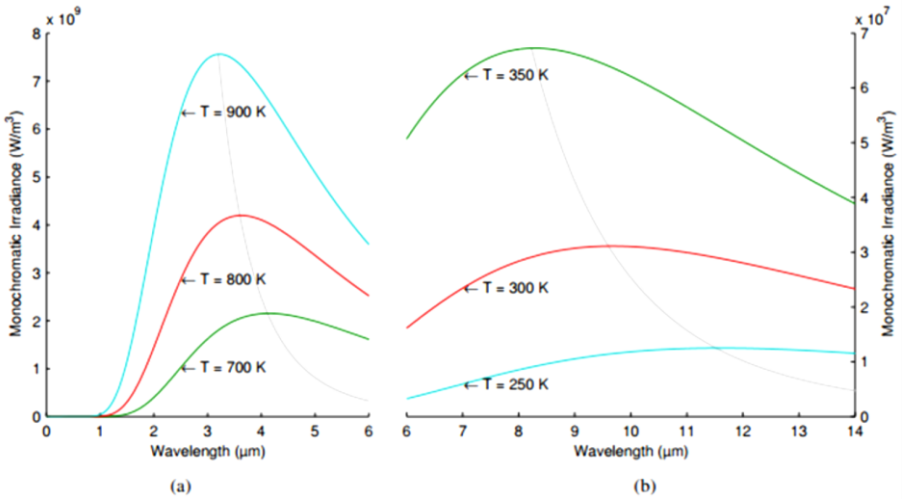

Figure 2. Radiation emitted by a blackbody according to Planck's Law.

$$\varepsilon_\lambda = \frac{\dot{Q}_{rad,\lambda}}{\dot{Q}_{rad,B,\lambda}} = \frac{\dot{Q}_{rad}}{\dot{Q}_{rad,B}} = \varepsilon \quad (4)$$

In addition, the surroundings must also be taken as an additional factor. In general, there are three ways by which the radiant energy striking an object may be dissipated: absorption, transmission and reflection [17]. The fractions of the total radiant energy that are associated with each of these modes of dissipation are respectively referred to as the body's absorptivity α, transmissivity τ and reflectivity ρ and are dependent on the wavelength [14]. The sum of these three parameters must be one at any wavelength, as given in Eq. (5).

$$\alpha + \tau + \rho = 1 \quad (5)$$

For blackbodies, the transmissivity and the reflectivity are equal to zero and all the radiant energy is absorbed. In the case of opaque materials, the radiant energy is only either absorbed or reflected and Eq. (5) is simplified to Eq. (6). Also, for a body emitting and absorbing thermal radiation in thermodynamic equilibrium, the emissivity is equal to the absorptivity.

$$\rho = 1 - \alpha = 1 - \varepsilon \quad (6)$$

Calculating the radiative heat transfer between groups of objects requires the solution of a set of simultaneous equations using the radiosity method [18]. In these calculations, the geometrical configuration of the problem is simplified to a set of numbers called view factors, $F_{i\to j}$, which give the proportion of radiation leaving any given surface that hits another specific surface. For a grey body with only two surfaces, the heat transfer is equal to:

$$\dot{Q} = \frac{\sigma(T_1^4 - T_2^4)}{\frac{1-\varepsilon_1}{A_1\varepsilon_1} + \frac{1}{A_1 F_{1\to 2}} + \frac{1-\varepsilon_2}{A_2\varepsilon_2}} \quad (7)$$

The radiation received by an IR camera lens comes from three different sources. The camera receives radiation from the target object, plus radiation from its surroundings that has been reflected onto the object's surface. Both of these radiation components are dampened when passing through a medium, such as air which, by absorbing part of the radiation, emits radiation itself [19]. This phenomenon is well acknowledged and is still an active field of investigation.

Errors in Thermographic Images of Known Heat Sources

Ball et al. [20] conducted rigorous investigations of errors that can affect thermographic images under controlled environments for volcanology. They mentioned that temperatures derived from remotely sensed infrared data are subject to errors due to the following conditions:

- Atmospheric attenuation by atmospheric scattering caused by particulate material in the atmosphere and absorption by gases;
- Instrument error from instrument noise, drift and systematic offsets in the sensor;
- Incorrect or unknown emissivity of the target where emissivity is defined as the ratio of the theoretical maximum (blackbody) radiance to the radiance of the surface at a given temperature;
- Errors arising from viewing the surface at an oblique angle; and;
- Integrated averaging of radiance over increasing pixel areas due to increased viewing distance (decreased resolution).

They conducted controlled experiments to investigate each of the factors mentioned above and had related it to field measurements in the field of volcanology. Their investigation did not consider reflectance errors arising from the presence of a heat source near a thermally reflecting surface such as that seen in Fig. 3. It can be noted that the reflectivity of a small portion of the copper block at an angle is more thermally reflective than the glass in the IR spectrum.

(a) (b)

Figure 3. Reflection error (a) visible light image (b) thermal image showing reflection errors.

These errors are often avoided by choosing an angle at which the thermal camera does not see interfering reflections, but this is not always possible.

The blurry areas in Fig. 3 (b) should be isothermal surfaces but instrument error causes some temperature deviation. The right side of Fig. 3(b) has an average temperature of 17.7 $^\circ C$ with respective maximum and minimum readings of 18.4 and 17 $^\circ C$. The true room and wall temperature was measured with a temperature reading of 17.2 $^\circ C$. We can obtain the correct wall temperature by adjusting the emissivity but the hand temperature readings would be incorrect. Changing the emissivity will still not give the known uniform temperature reading.

Emissivity can only be set once for the thermographic camera used and was set to 0.98 (the typical emissivity for a person's skin) for Fig.3 (b). It captures the right temperature reading with an average of 32.9 $^\circ C$ for most part, but suffers the problem of decreased resolution where the boundary of the hand ends. The reflection in the mirror had an average of 19.7 $^\circ C$ where, in fact, thermocouple measurements indicate

that is was 17.2 $^{\circ}C$. The shape, although not fully distinguishable, is clearly the reflection of a person's hand.

We hypothesize that if the objects in the scene were properly identified and captured with a better resolution, the temperature measurements could be improved. However, the price difference in available thermographic cameras is much higher compared to the increase in pixel density. The thermographic cameras used have a built-in digital camera and Multi Spectral Dynamic Imaging (MSX) [21] but could only provide a more detailed background of the thermographed scene with resolution close to the screen resolution. Thus, we attempted to augment the thermal data obtained by the camera in a relatively cheaper and higher resolution system capable of obtaining 3D depth information. Since this is our first study of the proposed system, we limited our scope with prior knowledge of an isothermal background, that is, all of the objects are held at a constant temperature while an object with a known temperature is identified and assigned the average temperature. The errors caused by the heated object can be evaluated without excessive radiation computations since we have verified that the affected areas are still at the background temperature.

Kinect System

The Kinect was originally designed by Microsoft as a motion sensing input device for gaming consoles [22]. First introduced in 2010, the release of its standard development kit (SDK) enabled technology enthusiasts and researchers to apply it to a more diverse range of applications [23]. It uses an infrared projector, a camera and a special microchip to implement a 3D scanning system based on structured light coding which is a variant of image-based 3D reconstruction. Depth is obtained using an infrared laser projector combined with a monochrome CMOS sensor, which captures video data under any light conditions and can be integrated in the output file as an RGBD data set. The sensing range of the depth sensor is adjustable, with the Kinect software automatically calibrating the sensor based on the environment. Although the Kinect's main innovation is its advanced gesture, facial and motion analysis, its contribution for depth determination is truly noteworthy. This study used the 2nd generation Kinect, which features higher resolution cameras (color camera: 1920×1080 at 30 fps; IR camera: 512×424), and a bigger field of view (70° horizontal FOV and 60° vertical FOV). Since the thermographic camera has smaller camera resolution and FOV, the captured thermal image is sufficiently located within the RGBD image captured by the Kinect system. We sought to use feature recognition from the visual image captured in the thermal camera to approximately match the captured scene with the RGBD image in the Kinect system. This approach will be further improved in the future to include the intrinsic parameters of the Kinect system and thermographic camera.

Experimental Set-Up and Results

The set-up, as shown in Fig. 4 is composed of a Forward Looking Infrared (FLIR) camera (FLIR E4) with an IR resolution of 80×60 pixels, a thermal sensitivity of less than 0.15 $^{\circ}C$, a field of view of $45^{\circ} \times 34^{\circ}$ and an uncooled microbolometer detector. It has a working temperature range of -20 $^{\circ}C$ to 250 $^{\circ}C$ with a calibrated accuracy of 2 $^{\circ}C$ or $\pm$ 2%, whichever is higher. The Kinect system is mounted together with the camera where the FOV of the thermal camera is a small portion of the scene captured by the Kinect system.

All components are connected to a computer located far from the camera's field of view to avoid unnecessary interference. The thermographed scene is composed of an isothermal environment, a 40cm copper cube and an aluminum surface. Aluminum was chosen since it is thermally opaque and had a low emissivity, resulting in high reflectivity. Aluminum can also be differentiated from the surroundings by the Kinect system. Some insulating foams were also used to minimize other unwanted thermal radiation sources. The temperatures of the environment, the reflecting surface and the copper cube were measured, monitored and logged with a T-type thermocouple and a Yokogawa MX100 data logger. The copper cube was heated in a sufficiently distant hotplate to around 60 $^{\circ}C$ and was placed on the table at the start of the experiment. The original thermal image on the area of the aluminum had an average reading of 34.97 $^{\circ}C$ and the area on which the copper was identified had a reading of 57.36 $^{\circ}C$ Spot thermocouple measurements respectively showed readings of 22.3 $^{\circ}C$ and 60.5 $^{\circ}C$ for the aluminum and copper.

Figure 4. Experimental set-up.

The acquired visible image and thermographic image from the FLIR camera are respectively shown in Figs.

5(a) and 5(b). It can be seen that there is a difference in the field of view of the visible and thermographic image. Figure 5(c), on the other hand, shows the visible light image obtained from the Kinect system containing the scene from the thermal image as approximated by the red box. The depth map, as seen in Fig. 5(d), also contains the thermographed scene with the features of the copper block and aluminum surface already detected. The next step was to perform image registration on all images using the pertinent features from all images. The thermal image was rescaled since its resolution was relatively small. We performed image registration based on the edge features of the copper and aluminum block.

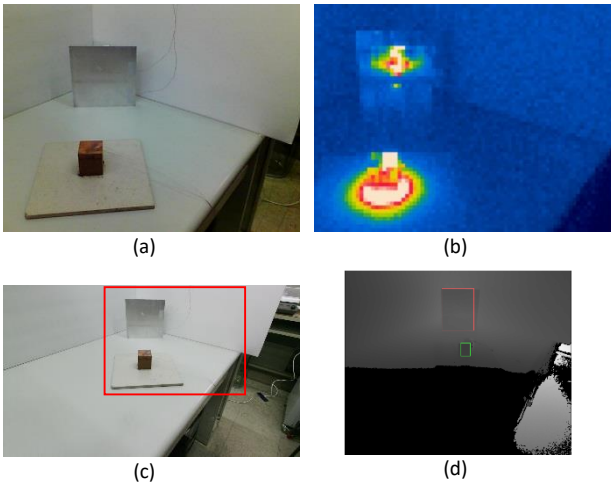

(a) (b) (c) (d)

Figure 5. Obtained images (a) from the built in visible camera of the FLIR camera; (b) thermal image from the FLIR camera; (c) visible image from the Kinect system with the bounding box approximating the FOV of the thermal camera; (d) reconstructed depth map from the Kinect system with the bounding box for the aluminum and copper blocks.

After all the images were matched, a depth-based correction was performed based on the surface energy balance from the aluminum. A simplification of the problem and the variables used is presented in Fig. 6.

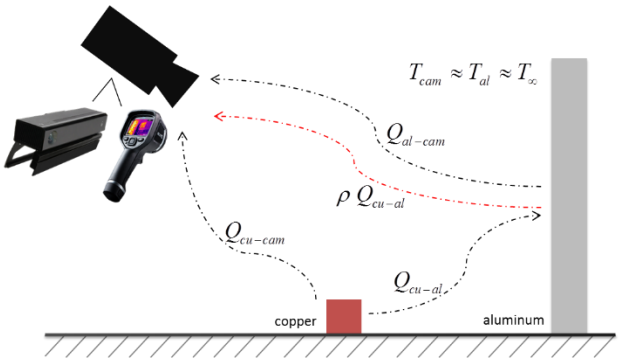

Figure 6. Assumptions and simplifications for the experimental case.

We hypothesized that the reflection error is not well accounted for in the thermal camera since it is perspective-dependent. The perceived thermal reading from the aluminum surface is approximated as:

$$Q_{al_{total}} = Q_{al-cam} + \rho_{al} Q_{cu-al} \tag{8}$$

where $Q_{al_{total}}$ is the total radiation received in the IR camera; Q_{al-cam} is the radiation emitted from the aluminum plate to the IR camera, which represents the true temperature of the aluminum plate; Q_{cu-al} is the radiation reflected from the copper to the aluminum and received by the IR camera, which will cause incorrect reading of the temperature level of the aluminum plate; ρ_{al} is the reflectivity of the aluminum. Definitions from Eq. (6) and a variation of Eq. (7) are used to expand Eq. (8) to Eq. (9):

$$\begin{aligned} &A_{al}\varepsilon_{al}F_{al\to cam}\sigma(T^4_{al_{fake}} - T^4_{cam}) = \\ &A_{al}\varepsilon_{al}F_{al\to cam}\sigma(T^4_{al} - T^4_{cam}) \\ &-(1-\varepsilon_{al})(A_{cu}\varepsilon_{cu}F_{cu\to al})(T^4_{cu} - T^4_{al}) \end{aligned} \tag{9}$$

which can be simplified as Eq. (10) to solve for the true aluminum temperature.

$$T_{al} = \left[\frac{\varepsilon_{al}T^4_{al_{fake}} + A\times T^4_{cam} - B\times T^4_{cu}}{A-B}\right]^{1/4} \tag{10}$$

where

$$A = A_{al}\varepsilon_{al}F_{al\to cam} \tag{11}$$

$$B = (1-\varepsilon_{al})(A_{cu}\varepsilon_{cu}F_{cu\to al}) \tag{12}$$

In the above equations, A_{al} and A_{cu} respectively represent the inspection area of the aluminum plate and copper; ε_{al} and ε_{cu} are the emissivities of aluminum and copper, respectively; T_{cam} is the temperature of the IR camera; and T_{cu} is the temperature of the copper, which can be measured from the IR camera. $T_{al_{fake}}$ is the temperature reading for the aluminum on the thermal camera without the correction and T_{al} is the corrected aluminum temperature. The view factors, $F_{i\to j}$, are computed based from geometric relations and distances acquired from the Kinect system. Different emissivities are assigned to both copper and aluminum based from [24] after they are identified. Figure 7 shows the the result of the depth-based correction considering the area calculations.

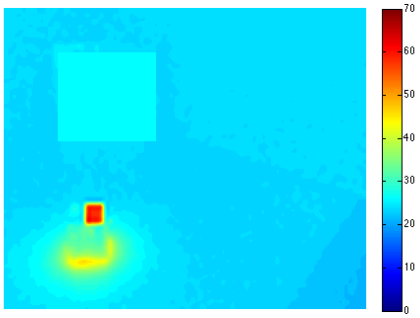

Figure 7. Thermal image after the depth based correction.

The corrected temperature for the aluminum surface was computed at an average temperature of 25.57

$^{\circ}C$, which is closer to the thermocouple reading of 22.3 $^{\circ}C$. The higher calculated readings may be related to the assumptions for the emissivity of the materials. Also, since we use an area-averaged correction for the aluminum, the noise present in the adjacent areas are more pronounced. The thermal image also shows a significant increase in resolution.

Conclusion

This paper discusses errors in temperature measurement using a thermographic camera under a known heat source. Experiments were carried out under the assumption that all other surfaces are isothermal. A Kinect system was used to detect objects in the scene and obtain depth data. Thermal data was then registered into the cloud points and depth-based correction was used to determine the object's average temperature. This scheme increased the accuracy of the temperature measurements obtained by a low-resolution thermographic camera. The accuracy of the correction scheme can be further enhanced by improving the pixel-to-pixel correspondence and computation of the relevant geometric parameters in the error correction algorithm. Obtaining the geometric features of the Kinect system's blind side can also be addressed.

Acknowledgment

The authors gratefully appreciate support from the Ministry of Science and Technology, Taiwan (grants MOST 103-2221-E-033-015 and MOST 104-2218-E-033-013); the Research Center for Microsystem Engineering at Chung Yuan Christian University, Taiwan; and the Center for Robotics Research at Chung Yuan Christian University, Taiwan.

References

[1] R. Gade and T. B. Moeslund, "Thermal cameras and applications: a survey," *Machine vision and applications*, vol. 25, no. 1, pp. 245-262, 2014. doi: 10.1007/s00138-013-0570-5

[2] R. DeMarines and B. Botwin, "Defense Industrial Base Assessment: U.S. Imaging and Sensors Industry," U.S. Department of Commerce, Washington, D.C., NW, 2006.

[3] P. Saunders, "How good is Quantitative Thermal Imaging?" *Automation and control*, vol. 2005, p. 19, 2005.

[4] C.-Y. Chen, C.-H. Yeh, B.-R. Chang, and J.-M. Pan, "3D Reconstruction from IR Thermal Images and Reprojective Evaluations," *Mathematical Problems in Engineering*, vol. 2015, p. 520534, 2015. doi: 10.1155/2015/520534

[5] M. A. de Souza, I. J. Sanches, and H. R. Gamba, "A new method for generating 3d thermography models," *Biomedical Engineering*, vol. 2012, p. 764081, 2012. doi: 10.2316/P.2012.764-081

[6] Y. M. Ng and R. Du, "Reconstruction of 3D thermal distribution from infrared images," in proceeding of *First Asian International Symposium on Mechatronics*, Xi'an, China, Sep., 2004, pp. 379-383.

[7] H. Xiao, Y. Zhang, and A. Wang, "Multispectral three-dimensional digital infrared thermal imaging," *Optical Engineering*, vol. 42, no. 4, pp. 906-912, 2003. doi: 10.1117/1.1557175

[8] E. Barker, X. P. Maldague, and D. Laurendeau, "Shape reconstruction from a single thermal image," *Optical Engineering*, vol. 34, no. 1, pp. 154-159, 1995. doi: 10.1117/12.195237

[9] J.-F. Pelletier, X. Maldague, "Shape from heating: a two-dimensional approach for shape extraction in infrared images," *Optical engineering*, vol. 36, no. 2, pp. 370-375, 1997. doi: 10.1117/1.601210

[10] S. Prakash, P. Y. Lee, and A. Robles-Kelly, "Stereo techniques for 3D mapping of object surface temperatures," *Quantitative Infrared Thermography Journal*, vol. 4, no.1, pp. 63-84, 2007. doi: 10.3166/qirt.4.63-84

[11] R. Yang and Y. Chen, "Design of a 3-D infrared imaging system using structured light," *IEEE Transactions on Instrumentation and Measurement*, vol. 60, no. 2, pp. 608-617, 2011. doi: 10.1109/TIM.2010.2051614

[12] M. Modest, *Radiative heat transfer*. Oxford: Academic Press, 2013.

[13] J. L. Miller, *Principles of infrared technology.* MA:Springer, 1994.

[14] J. R. Howell, R. Siegel, and M. P. Menguc, *Thermal radiation heat transfer*, CRC press, 2011.

[15] R. Usamentiaga, P. Venegas, J. Guerediaga, L. Vega, J. Molleda, and F. G. Bulnes, "Infrared thermography for temperature measurement and non-destructive testing," *Sensors*, vol. 14, pp. 12305-12348, 2014. doi: 10.3390/s140712305

[16] N. Utami, Y. Tamsir, A. Pharmatrisanti, H. Gumilang, B. Cahyono, and R. Siregar, "Evaluation condition of transformer based on infrared thermography results," in proceeding of *IEEE 9th International Conference on the Properties and Applications of Dielectric Materials*, Harbin, China, June 19, 2009, pp. 1055-1058. doi: 10.1109/ICPADM.2009.5252449

[17] K. Mollmann, D. Karstadt, F. Pinno, and M. Vollmer,

"Selected critical applications for thermography: Convections in fluids, selective emitters and highly reflecting materials," in proceeding of *Infrared Camera Calibration Conference*, 2005, pp. 161-173,.

[18] F. X. Sillion and C. Puech, *Radiosity and global illumination*, Springer, 1994.

[19] *The Ultimate Infrared Handbook for R&D Professionals*, FLIR® Systems, Inc., Wilsonville, OR.

[20] M. Ball and H. Pinkerton, "Factors affecting the accuracy of thermal imaging cameras in volcanology," *Journal of Geophysical Research: Solid Earth* (1978–2012), vol. 111, no. B11, 2006.

[21] S. HOCER, "Products focus," *Waste Management and Environment*, vol. 25, no. 6, pp. 39-40, 2014.

[22] D. DePriest and K. Barilovits, "LIVE: Xbox Kinect© s virtual realities to learning games," in proceeding of *TCC-Teaching Colleges and Community Worldwide Online Conference*, New York, NY, April 12, 2011, pp. 48-54.

[23] L. Cruz, D. Lucio, and L. Velho, "Kinect and RGBD images: Challenges and applications," in proceeding of *2012 25th SIBGRAPI Conference on Graphics, Patterns and Images Tutorials*, Minas Gerais, Brazil. Aug. 22, 2012, pp. 36-49.

[24] G. Blackwell, *The electronic packaging handbook*. Boca Raton, FL: CRC Press, 2000.